Supercapacitor energy storage system for fault ride-through of a DFIG wind generation system

A.H.M.A. Rahim [a,*], E.P. Nowicki [b]

[a] Department of Electrical Engineering, King Fahd University of Petroleum & Minerals, Dhahran, Saudi Arabia
[b] Department of Electrical & Computer Engineering, University of Calgary, Calgary, AB, Canada

ABSTRACT

The doubly fed induction generators (DFIGs) are preferred over other variable speed generators because of their advantages in terms of economy and control. One of the problems associated with high wind power penetration DFIG systems, however, is the inability of their converters to work properly under extreme low voltage conditions. This article presents a decoupled *P–Q* control strategy of a supercapacitor energy storage system, interfaced through a STATCOM, for low voltage ride through as well as damping enhancement of the DFIG system. The STATCOM meets the reactive power need under the depressed voltage condition, while the supercapacitor caters to the real power unbalance. An extensive dynamic model of the DFIG system including a supercapacitor DC–DC buck–boost converter and the STATCOM circuit has been developed. The fault ride-thorough capability of the generator has been investigated for a severe symmetrical three-phase to ground fault on the grid bus. Simulation results suggest that the proposed decoupled control of the supercapacitor STATCOM control strategy can help the DFIG ride through extreme low voltage conditions for significant duration. The proposed control strategy also damps the electromechanical transients, and thus quickly restores normal operation of the converters.

© 2012 Elsevier Ltd. All rights reserved.

1. Introduction

Among several fast growing wind turbine technologies, variable speed wind turbines utilizing doubly fed induction generators (DFIGs) are gaining popularity because of their higher energy transfer capability from wind, reduction of flicker by adjusting the shaft speed and flexible controls [1–3]. With such drive system wide range of variable speed constant frequency operation is possible with independent control capabilities of real and reactive power [4]. The stator of a wind turbine driven DFIG is directly connected to the grid while the rotor is connected through a back-to-back converter and a DC link capacitor. The frequency of the rotor injected voltage is adjusted depending on the turbine speed change to obtain constant frequency at the stator terminals [5,6]. Since the DFIG stator is directly connected to the grid via a step-up transformer and the rating of the grid-side and rotor-side converters is limited, the DFIG is quite sensitive to any grid disturbance [7]. Also, the existence of a sophisticated, multi-loop control structure of the converters makes the DFIG based wind power system prone to undesirable dynamic interaction with the grid [8].

Low voltage ride-through (LVRT) capability is of special interest in a wind power generator system that employs a doubly fed induction generator. LVRT grid code standards of power utilities

specify a minimum voltage profile that a wind farm should be able to ride-through. Although the operation of a DFIG wind turbine is satisfactory under balanced grid voltage conditions, there exists potential for a significant reduction in power output due to a low network voltage during grid disturbances. Under such conditions, the electromagnetic transients of the DFIG give rise to high over-currents to avoid disconnection in the semiconductors [9–11]. Different authors have reported solutions oriented to enhance fault ride-through capabilities. Many of these are based on implementing controllers in the rotor and grid side converters [11]. Some deal with reduction of high rotor inrush current observed during grid faults while others are based on limiting electromagnetic torque oscillations when a generator is subjected to a voltage dip [12]. The application of energy storage devices such as flywheel energy storage [13], superconducting magnetic energy storage [14,15] and battery energy storage [16] to smoothen wind power fluctuations have been reported. Capacitor energy storage for variable speed permanent magnet synchronous generators has been considered to damp out power oscillations [17]. Capacitor energy storage has also been reported to improve the voltage profile for fixed speed cage generators [18]. Storage of the excess energy of the generator during a low voltage condition and its utilization in the post-disturbance regime is suggested to improve the voltage profile [19]. Low voltage ride-through of permanent magnet synchronous generators with a current controlled voltage source converter was proposed in [20]. With increased wind penetration a variety of problems including voltage instability may require coordinated study on voltage control

and reactive power planning [21]. Since the power ratings of DFIG converters are generally not very large, and also because low voltage conditions may not allow the controllers located in the feedback circuit to act properly, additional short-duty energy storage devices installed at the DFIG terminals would be helpful.

Enhancement of DFIG system performance under low voltage conditions with additional real and reactive power support is considered in this article. A supercapacitor energy storage system interfaced through a STATCOM is used for this purpose. The organization of the article is as follows: Section 2 describes the model of the DFIG wind system. The STATCOM supercapacitor model is given in Section 3 followed by supercapacitor energy storage control design procedure in Section 4. Section 5 presents the simulation results and conclusions are drawn in Section 6.

2. DFIG wind turbine system model

Fig. 1 illustrates the DFIG wind power generation system connected to the grid through a step-up transformer and its transmission network. A back-to-back converter, consisting of two sub-converters VSC-1 and VSC-2, is connected in the rotor circuit. VSC-1, the grid-side converter, is connected to the generator stator through a transformer and filter circuit having resistance R_t and inductance L_t. The rotor side converter, VSC-2, is employed to control rotor voltage V_r whose frequency is adjusted according to the turbine speed so as to produce stator voltage V_s at the desired grid frequency. The supercapacitor controller is connected to the generator end of the transmission line. The models for the different components are given in the following [22].

2.1. The doubly fed induction generator

From the Park's transformation of the voltage–current–flux relationships of an induction machine operating under generator mode, the d–q components of stator and rotor currents can be expressed as,

$$\begin{bmatrix} i_{sd} \\ i_{rd} \end{bmatrix} = Z \begin{bmatrix} \omega_o R_s & 0 & \omega_e x_s & -\omega_e x_m \\ 0 & \omega_o R_r & -s\omega_o x_m & -s\omega_o x_m \end{bmatrix} [i_g] + \begin{bmatrix} \omega_o v_{sd} \\ \omega_o v_{rd} \end{bmatrix} \quad (1)$$

$$\begin{bmatrix} i_{sq} \\ i_{rq} \end{bmatrix} = Z \begin{bmatrix} \omega_e x_s & \omega_e x_m & \omega_0 R_s & 0 \\ s\omega_0 x_m & s\omega_0 x_r & 0 & \omega_o R_r \end{bmatrix} [i_g] + \begin{bmatrix} \omega_o v_{sq} \\ \omega_o v_{rq} \end{bmatrix} \quad (2)$$

Here the subscripts s and r stand for stator and rotor voltages (v) and currents (i) along the d–q axes. The state vector comprises of the d–q components of stator and rotor currents arranged as,

$i_g = [i_{sd}\ i_{rd}\ i_{sq}\ i_{rq}]'$. The matrix Z and slip s in the above, respectively, are given as,

$$Z = \begin{bmatrix} -x_s & -x_m \\ -x_m & -x_r \end{bmatrix}^{-1}, \quad s = \frac{\omega_o - \omega_r}{\omega_o} \quad (3)$$

The DFIG stator terminals always supply real power to the grid at sub-synchronous as well as super-synchronous speed. The rotor circuit delivers power to the grid at super-synchronous speed, while the grid supplies the rotor under sub-synchronous conditions. A list of symbols is given in the Nomenclature.

2.2. The electromechanical system

A two-mass model for the turbine generator system is adopted since a high inertia wind turbine is connected to a low inertia DFIG rotor with a relatively soft shaft. The dynamic equations of the two-mass representation are expressed as,

$$2H_t \frac{d\omega_t}{dt} = P_m - K_s \theta_s - D_t \Delta \omega_t \quad (4)$$

$$2H_g \frac{d\omega_r}{dt} = K_s \theta_s - P_e - D_g \Delta \omega_r \quad (5)$$

$$\frac{d\theta_s}{dt} = \omega_o (\omega_t - \omega_r) \quad (6)$$

In the above, θ_s is the shaft torsion angle, K_s is the shaft stiffness, H and D are the inertia and damping coefficients, respectively of turbine and generator; subscripts t and g refer to the turbine and generator quantities, respectively. The generator electrical output P_e is given as,

$$P_e = x_m i_{rq} i_{sd} - x_m i_{rd} i_{sq} \quad (7)$$

The mechanical power input to the generator supplied by the turbine is,

$$P_m = \frac{1}{2} \rho A C_p(\lambda, \beta) V_\omega^3 \quad (8)$$

Here ρ is the air density and A is the swept area by the turbine blades. The power coefficient C_p is expressed as a function of tip speed ratio λ and the blade pitch angle β [23],

$$C_p(\lambda, \beta) = 0.5176 \left(\frac{116}{\lambda_i} - 0.4\beta - 5 \right) e^{\frac{-21}{\lambda_i}} + 0.0068\lambda$$

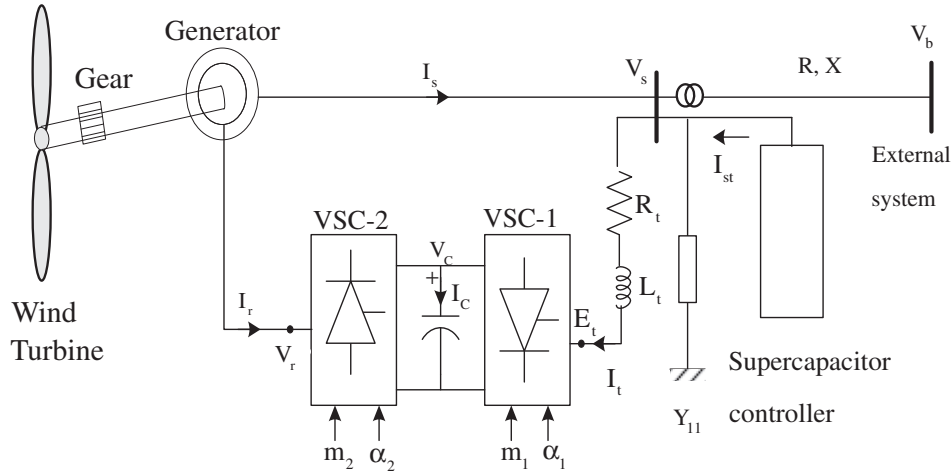$$\frac{1}{\lambda_i} = \frac{1}{\lambda + 0.08\beta} - \frac{0.035}{\beta^3 + 1} \quad (9)$$

Fig. 1. DFIG system configuration.

2.3. The converter system

Expressing the d–q components of the grid side converter current in the form $I_t = i_{td} + ji_{tq}$, the dynamic equations for the transformer- filter circuit can be written as,

$$\frac{d}{dt}\begin{bmatrix} i_{td} \\ i_{tq} \end{bmatrix} = \frac{\omega_o}{L_t}\begin{bmatrix} -R_t & (1-\Delta\omega_e)L_t \\ -(1-\Delta\omega_e)L_t & -R_t \end{bmatrix}\begin{bmatrix} i_{td} \\ i_{tq} \end{bmatrix} + \frac{\omega_o}{L_a}\begin{bmatrix} v_{sd} & -e_{tq} \\ v_{sq} & -e_{td} \end{bmatrix}$$

(10)

The currents and voltages are broken up in d–q quantities as, $I_t = i_{td} + ji_{tq}$, $V_s = v_{sd} + jv_{sq}$, and $E_t = e_{td} + je_{tq}$. Neglecting the converter losses, power balance gives the DC link voltage equation as,

$$\frac{dV_c}{dt} = \frac{1}{C}[m_1\cos\alpha_1 i_{td} + m_1\sin\alpha_1 i_{tq} + m_2\cos\alpha_2 i_{rd} \\ + m_2\sin\alpha_2 i_{rq}]$$

(11)

The grid-side and rotor-side voltages are related to the DC link voltage V_c through,

$$\begin{aligned} e_{td} = m_1 V_c\cos\alpha_1 \quad v_{rd} = m_2 V_c\cos\alpha_2 \\ e_{tq} = m_1 V_c\sin\alpha_1 \quad v_{rq} = m_2 V_c\sin\alpha_2 \end{aligned}$$

(12)

In the above, m_1, m_2, α_1, α_2 are the modulation indices (m) and phase angles (ψ) of the two converter voltages. Current supplied by the DFIG stator can be written as,

$$I_s = (V_s - V_b)Y_{12} + V_s Y_{11} + I_t - I_{st}$$

(13)

$Y_{12} = g_{12} + jb_{12}$ is the transmission line admittance (reciprocal of $R + jX$), $Y_{11} = g_{11} + jb_{11}$ is the local load admittance, V_b is the grid voltage, and I_{st} is the current injected by the STATCOM. Expressing the quantities in the stationary d–q reference frames, a relationships between the generator voltage bus voltage, generator current, and the STATCOM current is obtained as,

$$\begin{aligned} v_{sd}(g_{11} + g_{12}) - v_{sq}(b_{12} + b_{11}) = V_b g_{12} + i_{sd} - i_{td} + I_{std} \\ v_{sd}(b_{12} + b_{11}) + v_{sq}(g_{11} + g_{12}) = V_b b_{12} + i_{sq} - i_{tq} + I_{stq} \end{aligned}$$

(14)

3. The energy storage system model

3.1. The supercapacitor-STATCOM

Fig. 2 shows the connection diagram of the supercapacitor-STATCOM system connected to the generator terminals having voltage V_s. The STATCOM performs two tasks; it caters to the short term reactive need of the system and also acts as an interface for the supercapacitor. The supercapacitor is connected to the

STATCOM through a bi-directional DC–DC buck–boost converter. The operation of the buck–boost converter is controlled by varying the duty ratio through S_1 and S_2. The supercapacitor is modeled through an ideal capacitance (C_{sc}) and an equivalent series resistance (R_{sc}) as shown in the figure. R_{sc} accounts for resistive losses in the dielectric, plate material, and the electrolytic solution. The STATCOM current and voltage are related through,

$$L_{st}\frac{dI_{st}}{dt} + R_{st}I_{st} = V_{st} - V_s$$

(15)

where $V_{st} = mV_{DC}\angle\psi + \theta_s$, and $V_s = V_s\angle\theta_s$. V_{dc} is DC link voltage of the STATCOM; m and ψ are the modulation index and phase angle of the STATCOM converter, respectively. Expressing the STATCOM voltage along the synchronously rotating d–q frame coordinates and normalizing the quantities, (15) can be written as,

$$\begin{bmatrix} \dot{i}_{std} \\ \dot{i}_{stq} \end{bmatrix} = \begin{bmatrix} \frac{-\omega_o R_{st}}{L_{st}} & \frac{\omega_e}{\omega_o} \\ -\frac{\omega_e}{\omega_o} & \frac{-\omega_o R_{st}}{L_{st}} \end{bmatrix}\begin{bmatrix} I_{std} \\ I_{stq} \end{bmatrix} + \frac{\omega_o}{L_{st}}\begin{bmatrix} mV_{DC}\cos(\psi+\theta_s) - v_{sd} \\ mV_{DC}\sin(\psi+\theta_s) - v_{sq} \end{bmatrix}$$

(16)

Considering the converter to be lossless, the power balance equation will result in the capacitor voltage equation,

$$\frac{dV_{dcs}}{dt} = -\frac{m}{C_{dcs}}(I_{std}\cos(\psi+\theta_s) + I_{stq}\sin(\psi+\theta_s)) - \frac{I_{sc}}{C_{dcs}}$$

(17)

where I_{sc} is the supercapacitor current and C_{dcs} is the capacitance of the DC link.

Referring to Fig. 2, the supercapacitor current is related to the supercapacitor voltage V_{sc} through,
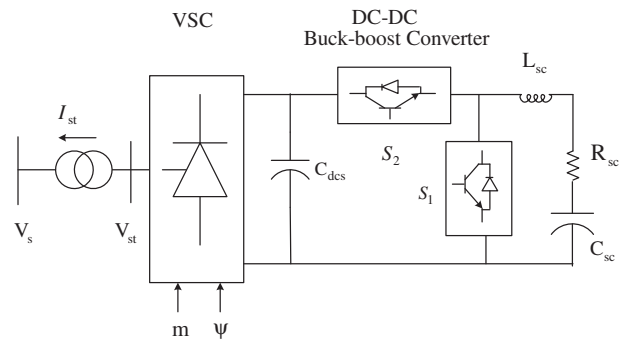

Fig. 2. Supercapacitor system connected to DFIG bus.

Fig. 3. DC–DC converter control system for supercapacitor storage.

$$V_{sc} = E_{sc} + R_{sc}I_{sc}; \quad I_{sc} = C_{sc}\frac{dE_{sc}}{dt} \tag{18}$$

3.2. Supercapacitor DC–DC converter control

The main circuit of the bidirectional DC–DC converter, shown in Fig. 2, contains three energy storage components, the DC link capacitor (C_{dc}), the choke (L_{sc}) and the super capacitor (C_{sc}). The DC converter control system is shown in Fig. 3. The DC link voltage (V_{dc}) is compared to the reference $\left(V_{dc}^{ref}\right)$ and the error is taken to drive the PI voltage controller which outputs the reference current I_{sc}^{ref}. The voltage reference for the converter is obtained as the sum of supercapacitor voltage V_{sc} and the inductor voltage reference V_L^{ref} obtained from the current loop PI controller. The main objectives of the control are to regulate the DC-link voltage with energy stored in the supercapacitor, and to keep the supercapacitor voltage V_{sc} in its desired operating range.

The voltage and current controllers in Fig. 3 are simple PI devices and the controller dynamic relationships are,

$$\left(V_{DC}^{ref} - V_{DC}\right)\left(k_{pv} + \frac{k_{iv}}{s}\right)\left(\frac{1}{1 + \tau_{sc}s}\right) = I_{sc}^{ref} \tag{19}$$

$$\left(I_{sc}^{ref} - I_{sc}\right)\left(k_{pi} + \frac{k_{ii}}{s}\right) = V_L \tag{20}$$

The controller parameters are obtained following the procedure outlined in [24].

4. Decoupled supercapcitor STATCOM control

At steady state, the supercapacitor STATCOM system is considered to be floating without affecting any power flow to and from the supercapacitor. Variation from the steady condition, as detected by a change in generator terminal voltage magnitude and angle, initiates the STATCOM operation. The expressions for real and reactive power flow through the STATCOM can be written as,

$$P_{st} = V_sI_{std}\cos\theta_s + V_sI_{stq}\sin\theta_s$$
$$Q_{st} = V_sI_{std}\sin\theta_s - V_sI_{stq}\cos\theta_s \tag{21}$$

By transforming the STATCOM current through the relationship, $I_{st}^{new} = I_{st}e^{-j\theta_s}$, or writing,

$$I_{std}^{new} = I_{std}\cos\theta_s + I_{stq}\sin\theta_s$$
$$I_{stq}^{new} = I_{stq}\cos\theta_s - I_{std}\sin\theta_s \tag{22}$$

and substituting (22) in (21), a set of decoupled relationships of real and reactive power of the STATCOM can be obtained as,

$$P_{st} = V_sI_{std}^{new}; \quad Q_{st} = -V_sI_{stq}^{new} \tag{23}$$

With the transformed STATCOM currents of (22), Eq. (16) can be expressed as [18],

Fig. 4. Decoupled control strategy for the storage system.

$$\frac{d}{dt}\begin{bmatrix} I_{std}^{new} \\ I_{stq}^{new} \end{bmatrix} = \omega_b\begin{bmatrix} -\frac{R_{st}}{L_{st}} & 0 \\ 0 & -\frac{R_{st}}{L_{st}} \end{bmatrix}\begin{bmatrix} I_{std}^{new} \\ I_{stq}^{new} \end{bmatrix} + \begin{bmatrix} r_1 \\ r_2 \end{bmatrix} \tag{24}$$

Here

$$\begin{bmatrix} r_1 \\ r_2 \end{bmatrix} = \omega_b\begin{bmatrix} \frac{\omega}{\omega_b}I_{stq}^{new} + \frac{mV_{DC}}{L_{st}}\cos\psi - \frac{V_s}{L_{st}} \\ -\frac{\omega}{\omega_b}I_{std}^{new} + \frac{mV_{DC}}{L_{st}}\sin\psi \end{bmatrix} = \omega_b\begin{bmatrix} \frac{\omega}{\omega_b}I_{stq}^{new} + \frac{e_{xd}}{L_{st}} - \frac{V_s}{L_{st}} \\ -\frac{\omega}{\omega_b}I_{std}^{new} + \frac{e_{xq}}{L_{st}} \end{bmatrix} \tag{25}$$

From (25) one obtains,

$$e_{xd} = \frac{L_{st}}{\omega_b}\left(r_1 - \omega i_{stq}^{new}\right) + V_s \quad e_{xq} = \frac{L_{st}}{\omega_b}\left(r_2 + \omega i_{std}^{new}\right) \tag{26}$$

$$m = \frac{\sqrt{e_{xd}^2 + e_{xq}^2}}{V_{DC}} \quad \text{and} \quad \psi = \tan^{-1}\left(\frac{e_{xq}}{e_{xd}}\right)$$

Eq. (24) shows that transformed currents I_{std} and I_{stq} are excited by r_1 and r_2 respectively, through a simple first-order relationship and with no cross-coupling. The control rule (26) is thus completed by defining the feedback loops and PI controllers as follows:

$$r_1 = \left(k_{p1} + \frac{k_{i1}}{s}\right)\left(I_{std}^* - I_{std}\right)$$
$$r_2 = \left(k_{p2} + \frac{k_{i2}}{s}\right)\left(I_{stq}^* - I_{stq}\right) \tag{27}$$

The decoupled control algorithm can be expressed through the block diagram of Fig. 4.

5. Simulation results

Most wind generators, particularly the DFIG, are sensitive to low voltage conditions at the generator terminals. Since during grid faults reactive support cannot reach past the faulted point, generators would speed up beyond the set limits necessitating off-line tripping. Various utilities around the globe have come up with grid codes for low voltage ride-through [LVRT] standards for large wind plants. The allowable low voltage duration in many countries are in the range of 100–250 ms (United Kingdom 140 ms, Denmark 100 ms, Belgium 200 ms, Germany 150 ms, Nordel 250 ms, Hydro-Quebec 150 ms) with voltage ranges of 0–25% of normal value, and recovery time of 0.8–3 s. However, certain utilities in the USA, Italy, and some parts of Canada have higher recommended low voltage durations [25].

The dynamic performance of the DFIG system given in Fig. 1, particularly its behavior when subjected to a very low voltage, is investigated by applying symmetrical three phase faults of various durations at the grid bus with zero fault impedance. Under steady state conditions, the doubly fed generator supplies 0.9 pu power at

terminal voltage of 1.05 pu. When the system is subjected to low voltage, the system dynamic performance deteriorates giving rise to oscillations. The system variables remain within acceptable limits for fault durations of up to 120 ms, beyond which there is total voltage collapse. In this article we present the results for a 250 ms symmetrical fault at the grid bus. A 250 ms three-phase to ground fault at the grid is a particularly intense disturbance compared to the critical case (120 ms). The dynamic responses are compared for the cases with and without the proposed supercapacitor STATCOM decoupled control strategy. The parameters of the DFIG and supercapacitor STATCOM system are given in the Appendix A. The values of the drive-train parameters are taken from Akhmatov [26].

Figs. 5–8 show the variations of induction generator terminal voltage, power output, speed and the stator current variations for a three phase to ground fault of 250 ms duration at the grid bus. In the absence of supercapacitor STATCOM control the generator terminal voltage falls steeply as shown in Fig. 5 and the power output becomes virtually zero (Fig. 6). This causes the machine to accelerate rapidly and the rotor speed continues to grow as shown in Fig. 7. The drastically reduced voltage at the generator stator and rotor circuits pushes the generator armature current to a very large value (Fig. 8). Examination of the stator current response without supercapacitor energy storage control indicates the possibility of stator current reaching as high as 2.5 pu. Moreover, there is significant harmonic content in the stator current.

The response recorded with the proposed decoupled P–Q control of the supercapacitor STATCOM energy storage unit shown in Fig. 5 (solid line) indicates that the generator terminal voltage is maintained near the normal value even during the fault. The post fault oscillations in the power output, generator speed and stator current are effectively removed by the supercapacitor control as can be seen in Figs. 6–8. Normal operating conditions are restored in less than 5 s.

The core function of the proposed control operation in the DFIG system is to maintain a constant DC-link capacitor voltage. Since the generator terminal voltage becomes significantly depressed for a severe low voltage condition at the point of common coupling, the converter DC-link voltage progressively falls without the supercapacitor control as shown in Fig. 9. This, in turn, causes malfunction in the converter circuitry controls and hence causes the over-currents in the system. It can be observed in Fig. 9 that the proposed decoupled controller smoothly raises the DC-link voltage slightly above 1 pu.
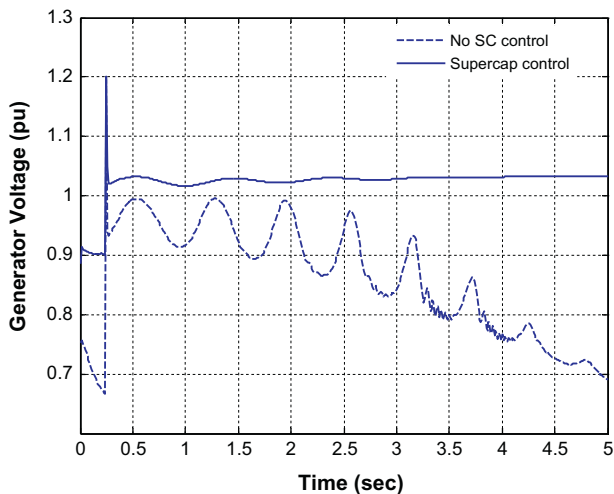

Fig. 6. DFIG power output variations following a 250 ms symmetrical three-phase to ground fault corresponding to Fig. 5.

Fig. 7. DFIG rotor speed variations following a 250 ms three-phase to ground fault on the grid bus, with and without additional supercapacitor control.

Fig. 5. DFIG terminal voltage following a 250 ms three-phase to ground fault at the grid bus, with and without additional supercapacitor control.
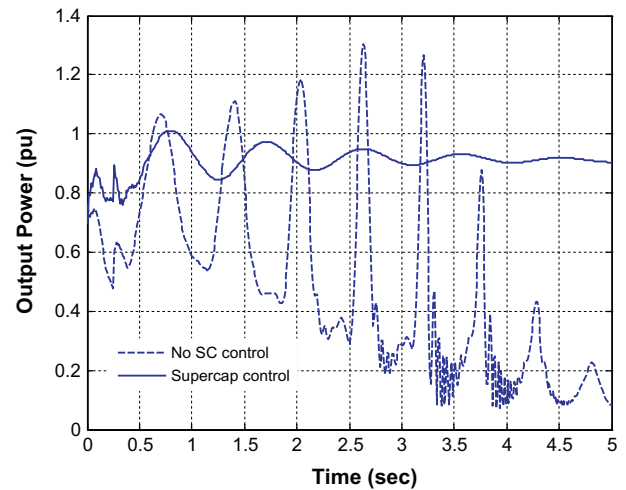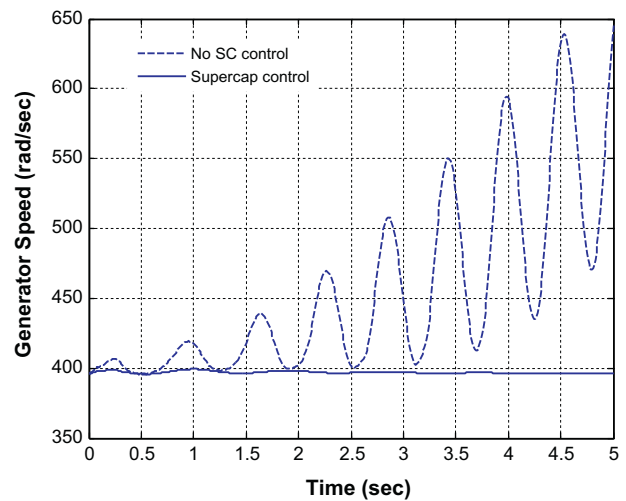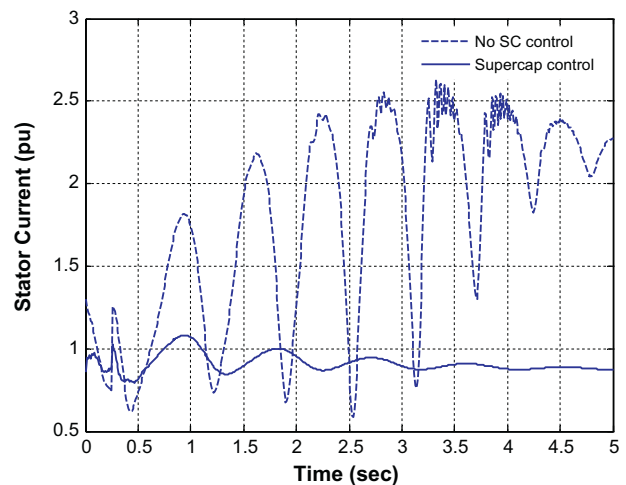

Fig. 8. DFIG stator current variation following a 250 ms three-phase to ground fault at the grid, with and without additional supercapacitor control.
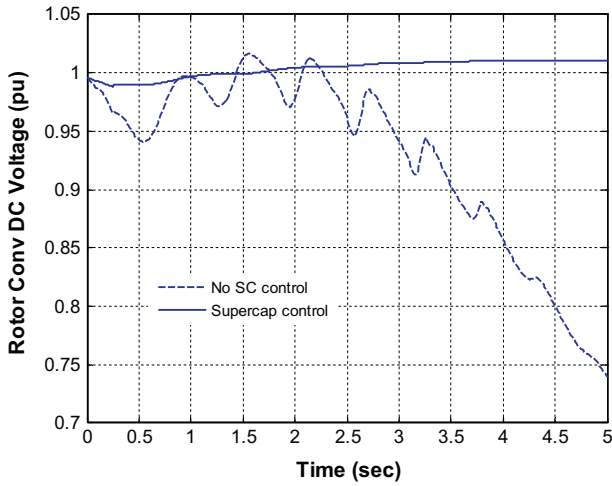
Fig. 9. DC capacitor voltage variation of the DFIG following a 250 ms three-phase to ground fault on the grid bus.
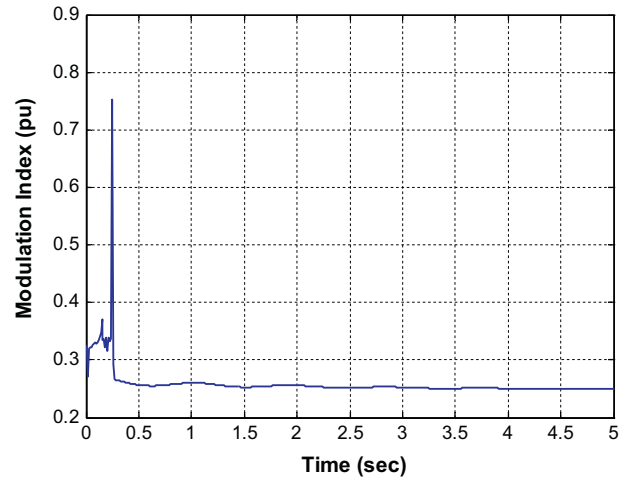

Fig. 12. Modulation index of the STATCOM voltage following a 250 ms three-phase to ground fault on the grid bus, with supercapacitor control.
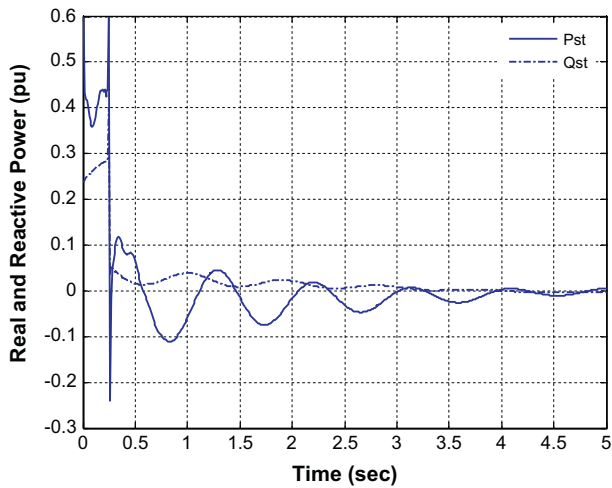

Fig. 10. Real and reactive power supplied by the supercapacitor STATCOM energy storage system following a 250 ms symmetrical three- phase fault to ground at the grid bus.
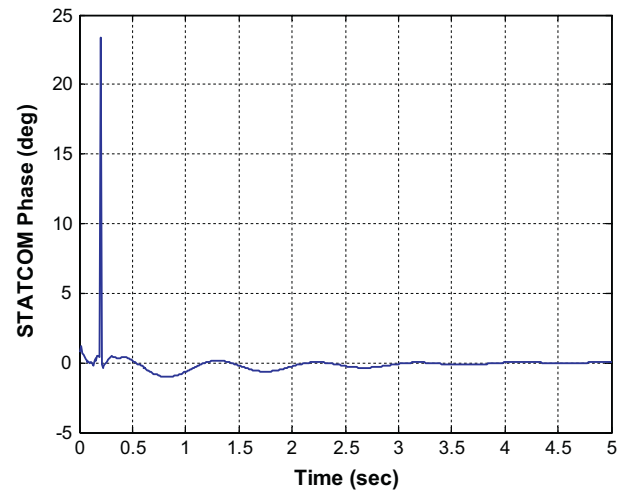

Fig. 13. Phase angle of the STATCOM voltage following a 250 ms three-phase to ground fault with supercapacitor control.

The variations of real and reactive power supplied by the supercapacitor STATCOM energy storage device are shown in Fig. 10. During the fault, the supercapacitor absorbs the excess generator power. The supercapacitor at that stage acts as a load. As the system condition changes, supercapacitor energy flow alternate between receive and supply modes as is indicated in the figure. The DC link voltage of the STATCOM, shown in Fig. 11, plays an important role in real and reactive power exchange by keeping its voltage more or less constant during the transient period.

Figs. 12 and 13 show the variations of modulation index (m) and phase angle (ψ) of the STATCOM voltage when the decoupled P–Q controls are activated through the energy storage devices. It can be seen that aside from the spike at the time of fault clearing, the control excursions are very small for this severe low voltage condition. It indicates that the controller can tackle worse scenarios without risking saturation.

6. Conclusions

Enhancement of fault ride-through for a doubly fed induction generator wind generator system with the help of supercapacitor and STATCOM energy storage device is investigated in this article. A very detailed dynamic model of the system including the turbine,

Fig. 11. DC capacitor voltage of the STATCOM converter following a 250 ms three-phase to ground fault at the grid bus.

the generator, the DFIG converters, the buck–boost converters of the supercapacitor and the STATCOM has been employed to design the energy storage system control strategy. It has been observed that the proposed controller helps the DFIG to ride through severe low voltage conditions to the satisfaction of the grid codes established by the most electrical utilities. The STATCOM compensates for the reactive power unbalance in the system, thus helping the generator to ride through the low voltage condition. The supercapacitor meets the real power need, by absorbing or delivering power as required by the system, thus improving the damping profile. The amount of real and reactive power supplied by the supercapacitor and STATCOM, respectively, are not large and the excursions of the internal controls of the STATCOM are very low avoiding the possibility of saturation.

Acknowledgments

Appendix A

The parameter values are in per unit, *except stated otherwise.*

A.1. DFIG

r_s	0.00473	x_s	3.418	ρ	1.225 kg/m^3
r_r	0.024	x_r	3.418	Blade radius	13.5 m
R_a	1	x_m	3.289	Gear ratio	1:23
X_a	0.1	R	0.8	A	577 m^2
C	1	X	1	V_w	9 m/s
H_g	0.5 s	H_t	2.5 s	$D_g = D_t$	0
g_{11}	0.4023	b_{11}	0.0242		

A.2. STATCOM and supercapacitor

R_{st} = 0.01 pu	L_{st} = 0.15 pu	C_{dc} = 1 pu		
L_{sc} = 0.18	R_{sc} = 0.1	C_{sc} = 350	K_{pv} = 12.64	K_{iv} = 0.786
K_{pi} = 395.04	K_{ii} = 438780	τ_{sc} = 0.00028135		

References

[1] Gautam D, Vittal V, Harbour T. Impact of increased penetration of DFIG-based wind turbine generators on transient and small signal stability of power systems. IEEE Trans Power Syst 2009;24:1426–34.

[2] Mishra Y, Mishra S, Tripathy M, Senroy N, Dong ZY. Improving stability of a DFIG-Based wind power system with tuned damping controller. IEEE Trans Energy Convers 2009;24:650–60.

[3] Lin WM, Hong CM, Cheng FS. Design of intelligent controllers for wind generation system with sensorless maximum wind energy control. Energy Convers Manage 2011;52:1086–96.

[4] Qiao W, Venayagamoorthy GK, Harley RG. Real-time implementation of a STATCOM on a wind farm equipped with doubly fed induction generators. IEEE Trans Indust Appl 2009;45:98–107.

[5] Qiao W, Venayagamoorthy GK, Harley RG. Real-time implementation of a STATCOM on a wind farm equipped with doubly fed induction generators. IEEE Trans Indust Appl 2009;45:98–107.

[6] Miao Z, Fan L. The art of modeling and simulation of induction generator in wind generation applications using high-order model. Simul Model Pract Theory 2008;16:1239–53.

[7] Hu J, Nian H, Xu H, He Y. Dynamic modeling and improved control of DFIG under distorted grid voltage conditions. IEEE Trans Energy Convers 2011;26:163–75.

[8] Ostadi A, Yazdani A, Varma RK. Modeling and stability analysis of a DFIG-based wind-power generator interfaced with a series-compensated line. IEEE Trans Power Deliv 2009;24:1504–14.

[9] Meegahapola LG, Littler T, Flynn D. Decoupled-DFIG fault ride-through strategy for enhanced stability performance during grid faults. IEEE Trans Sustain Energy 2010;1:152–62.

[10] Lima FKA, Luna A, Rodriguez P, Watanabe EH, Blaabjerg F. Rotor voltage dynamics in the doubly fed induction generator during grid faults. IEEE Trans Power Electron 2010;25:118–30.

[11] Luna A, Lima FK, Santos D, Rodríguez P, Watanabe EH, Arnaltes S. Simplified modeling of a DFIG for transient studies in wind power applications. IEEE Trans Indust Electron 2011;58:9–20.

[12] Rahimi M, Parniani M. Coordinated control approaches for low-voltage ride-through enhancement in wind turbines with doubly fed induction generators. IEEE Trans Energy Convers 2010;25:873–93.

[13] Cardenas R, Pena R, Asher G, Clare J. Power smoothing in wind generation systems using a sensorless vector controlled induction machine driving a flywheel. IEEE Trans Energy Convers 2004;19:206–16.

[14] Nomura S, Ohata Y, Hagita T, Tsutsui H, Tsuji-Iio S, Shimada R. Wind farms linked by SMES systems. IEEE Trans Appl Supercond 2005;15:1951–4.

[15] Chen S-S, Wang L, Lee W-J, Chen Z. Power flow control and damping enhancement of a large wind farm using a superconducting magnetic energy storage unit. IET Renew Power Gener 2009;3(2009):23–38.

[16] Yang Z, Shen C, Zhang L, Crow ML, Atcitty S. Integration of a StatCom and battery energy storage. IEEE Trans Power Syst 2001;16:254–60.

[17] Muyeen SM, Takahashi R, Murata T, Tamura J. Integration of an energy capacitor system with a variable-speed wind generator. IEEE Trans Energy Convers 2009;24:740–9.

[18] Ahsanul Alam M, Rahim AHMA, Abido MA. Supercapacitor based energy storage system for effective eault ride through of wind generation system. In: IEEE international symposium on industrial electronics (ISIE-2010), Bari, Italy; July, 2010.

[19] Vinothkumar K, Selvan MP. Novel scheme of enhancement of fault ride through capability of doubly fed induction generator based wind farms. Energy Convers Manage 2011;52:2651–8.

[20] Muyeen SM, Al-Durra A, Tamura J. Variable speed wind turbine generator system with current controlled voltage source inverter. Energy Convers Manage 2011;52:2688–94.

[21] Amaris H, Alfonso M. Coordinated reactive power management in power networks with wind turbines and FACTS devices. Energy Convers Manage 2011;52:2575–86.

[22] Rahim AHMA, Habiballah IO. DFIG rotor voltage control for system dynamic performance enhancement. Electr Power Syst Res 2011;81:503–9.

[23] Heier S. Grid integration of wind energy conversion systems. 2nd ed. John Wiley & Sons Ltd.; 2007.

[24] Camara MB, Gualous H, Gustin F, Berthon A. Design and new control of DC/DC converters to share energy between supercapacitors and batteries in hybrid vehicles. IEEE Trans Veh Technol 2008;57:2721–35.

[25] Tsili M, Papathanassiou S. A review of grid code technical requirements for wind farms. IET Renew Power Gener 2009;3:308–32.

[26] Akhmatov V. Induction generators for wind power. MultiScience Publishing Company; 2005.